Published in Chem. Eng. Sci., 63, 5339-5251 (2008)

# Experimental Characterization and Population Balance Modelling of the Dense Silica Suspensions Aggregation Process

M. Tourbin, C. Frances[1]

*Université de Toulouse, Laboratoire de Génie Chimique CNRS/INPT/UPS UMR 5503,*
*5, rue Paulin Talabot, BP 1301, 31106 Toulouse Cedex 01, France*

## Abstract

Concentrated suspensions of nanoparticles subjected to transport or shear forces are commonly encountered in many processes where particles are likely to undergo processes of aggregation and fragmentation under physico-chemical interactions and hydrodynamic forces. This study is focused on the analysis of the behaviour of colloidal silica in dense suspensions subjected to hydrodynamic forces in conditions of destabilization.

A colloidal silica suspension of particles with an initial size of about 80 nm was used. The silica suspension concentration was varied between 3 and 20% of weight. The phenomenon of aggregation was observed in the absence of any other process such as precipitation and the destabilization of the colloidal suspensions was obtained adding sodium chloride salt.

The experiments were performed in a batch agitated vessel. The evolution of the particle size distributions versus time during the process of aggregation was particularly followed on line by acoustic spectroscopy in dense conditions. Samples were also analyzed after an appropriate dilution by laser diffraction. The results show the different stages of the silica aggregation process whose kinetic rates depend either on physico-chemical parameters or hydrodynamics conditions. Then, the study is completed by a numerical study based on the population balance approach. By the fixed pivot technique of Kumar and Ramkrishna (1996), the hypothesis on the mechanisms of the aggregation and breakage processes were justified.

[1]Corresponding author.
Christine.Frances@ensiacet.fr (C. Frances)

Finally, it allows a better understanding of the mechanisms of the aggregation process under flowing conditions.

*Keywords*: Colloidal Phenomena, Suspensions, Characterization, Particulate Processes, Agglomeration, Population balance.

## 1. Introduction

Many industrial applications involve nanoparticles. Their usual properties (optical properties, texture, rheological behaviour, bioavailability …), in the form of powders or suspensions, are closely associated to the particle size and to their dispersion state. Relating to the different methods of generation or treatment of nanoparticles suspended in a liquid phase (precipitation, filtration, wet grinding, …) an inherent problem is the difficulty of controlling the process of aggregation and then of preserving the quality and the stability of the products. The physicochemical properties of the medium and the hydrodynamic conditions (shear, transport flow, …) are decisive with regards to the aggregation phenomenon. So, it is essential to know the influence of these parameters in order to control and model the aggregation process during the generation or treatment steps.

The stability of the suspensions depends on the forces which control the movement of the particles. It can be the result of the relative movement of the particles by diffusion (Brownian movement) or be induced by an external force (shearing by agitation or flow) or be controlled by the gravitational and/or repulsive interparticle interactions (Israelachvili, 1992).

The aggregation of colloidal silica has yet been studied in a number of ways. Experimentally, the analysis of the evolution of the particle size and the formation of structured aggregates are usually made in diluted conditions or in concentrated conditions but off-line of the process. For example, Schaer et al. (2001) used the well known experimental technique of laser light diffraction to determine particle size distributions during an aggregation process in diluted conditions. Their analysis of the evolution of the PSD during silica aggregation allowed them to propose a description of the mechanisms of the aggregation process. Schantz Zackrisson et al. (2006) and Motoyoshi et al. (2005) followed the PSD during silica aggregation process by the technique of dynamic light scattering, which allows measuring submicronic sizes below

the limit of the static light diffusion and diffraction methods. As an example of qualitative study of the aggregation and gelation kinetics of colloidal silica, the works of Gruy (2001) and Trompette and Meireles (2003) show the contribution of turbidimetry mesurements. Small angle light scattering and rheological measurements were used by Wyss et al (2004) in more concentrated conditions to follow the silica aggregation process. The capabilities and limitations of several analytical techniques concerning the characterization of the size distribution of colloidal silica particles in suspension were detailed in a previous work (Tourbin and Frances, 2007). None of the systems studied was able to give a correct particle size distribution over the full range of concentration considered (≤ 30% wt.), but important information was obtained on the dispersed medium by the use of these different complementary methods:

- A mean diameter may be estimated from online analysis based on multiple light scattering for the entire concentration range studied.
- Photon correlation spectroscopy allows the measurement of the size distribution of particles in terms of hydrodynamic diameter from which the particle diameter can be derived by calculating the Debye length. By this technique, consistent particle size distributions were obtained for dilute suspensions ($\Phi < 0.43$ %).
- Using acoustic spectroscopy, it was concluded that the sound attenuation spectrum is a crude and pure response containing important information on the physical properties of particles in suspension like the size or the structure. In contrast to previous techniques, good analyses were possible by this method only for relatively concentrated silica suspensions ($\Phi > 0.43$ %).

It is well known that the evolution of the aggregates size distribution greatly depends on the nature of the particles and on the way the collisions occur. There are three main mechanisms of transport of the particles:

- the Brownian motion, that leads to a generally called “perikinetic” aggregation ;
- The fluid motion, that leads to a generally called “orthokinetic” aggregation ;
- The differential settling.

Concerning the flowing of nanoparticles, differential settling was neglected.

Several authors (David et al., 2003; Schaer, 1997) have evidenced the multiplicity of collision mechanisms and the existence of an efficiency factor for sticking, which is a function of the particle size, the hydrodynamic conditions, etc. For example, based on an experimental and numerical (using the moments method) study of the colloidal silica aggregation process, Schaer (1997) distinguished three successive steps of aggregation depending on the value of the particle or the aggregate size $d$:

- If $L_0 \leq d < L_{ar}$ (where $L_0$ was the minimal size of the particle and $L_{ar}$ the maximal size) the silica particles undergo a slow perikinetic aggregation which is the aggregation of primary particles between them. Concerning Ludox particles of 12 nm in diameter, the maximal size observed by Schaer during the slow perikinetic aggregation was about 250 nm.
- If $L_{ar} \leq d < \lambda_k$ (where $\lambda_k$ is the Kolmogorov micro-scale of the shear flow): the silica particles undergo a fast perikinetic aggregation which is the aggregation of aggregates between them or of aggregates with primary particles.
- If $d \geq \lambda_k$: the silica particles undergo a orthokinetic aggregation which is the aggregation of aggregates between them associated to a breakage process according to the shear conditions.

In another approach, Gruy (2001) studied the aggregation of silica micrometric powder in water by using Kuster’s approach (Kuster, 1991) for collision efficiency calculation and Brakalov’s approach (Brakalov, 1987) for aggregation-fragmentation dynamics at high time levels. Using Brownian and turbulent aggregation kernel, and a power law breakage kernel,

he modelled the silica optical properties and aggregation through the turbidity of the suspension, and using a fractal dimension and a limit size for the aggregates.

The objective of the present work is to reach a better understanding of the aggregation mechanisms of nanoparticles in dense conditions. For this purpose, two techniques of characterization of the particle size distributions which are based on completely different physical principles and experimental conditions for the analysis (on-line analyses in dense conditions by acoustic spectroscopy and off-line analyses in diluted conditions by laser light diffraction).

In the reported works, the particle size measurements were made in dilute conditions. The use of acoustic spectroscopy in real conditions of concentration allows verifying the impact of the dilution step. Indeed, the cohesion and the strength of the aggregates are revealed by the comparison of the results obtained by both techniques in this work. The agreement between the results also validates the numerous previous works realized in diluted conditions.

Then, the population balance modelling is also used to get a better comprehension of the aggregation process. In particular, the aim is to understand if the aggregation and breakage kernels commonly used are well-adapted to describe a real process and if they are a good manner to describe the evolution of the experimental particle size distributions.

## 2. Experimental study

### 2.1. Materials and methods

*Colloidal silica suspensions*

A colloidal silica suspension, Klebosol 30R50 (AZ Electronical Materials, France), having an initial solid content of 30% w/w was used. Its density is about 1.21 $g.cm^{-3}$ (silica density is 2.37 $g.cm^{-3}$) and its specific surface around 50 $m^2.g^{-1}$.

It was observed by scanning electronic microscopy that silica particles of Klebosol 30R50 were spherical and monodispersed. Their average number diameter was roughly estimated at 80 nm.

Deionized water (pH~6 and $\Lambda$~5-7 $\mu S$) was used to prepare diluted silica suspensions from the Klebosol 30R50 initial suspension. The solid content of these suspensions is determined with a precision of $10^{-2}$ %, by the measure of the humidity rate by thermogravimetry using a Halogen Moisture Analyser HB43 desiccation balance (Mettler Toledo).

The stability of the different silica suspensions was previously analyzed. Using dynamic diffusion of light, and with measurements of pH and zeta potential, it was established that the silica suspensions remain stable and homogeneous in the range of concentration used (3% < w/w < 20%). Moreover, the homogeneity of the suspensions is not affected by major destabilization phenomena such as particle migration (creaming, sedimentation), particle size variation or aggregation (coalescence, flocculation).

*Particle size distributions measurements*

In this study, the size of the suspended particles was measured by two different ways: laser light diffraction and acoustic spectroscopy.

On one hand, a Mastersizer 2000 (Malvern Instruments) was used to analyze the samples by laser light scattering in diluted conditions. To study the evolution of the properties of the suspension by laser light scattering, it is required to stop the aggregation of the removed sample. A method based on the maximal stability of the silica suspensions at pH 2 was developed by Schaer et al. (2001). It consists in a quenching of the aggregated suspensions

mixing the removed sample (1/5 v/v) and a buffer solution at pH 1.9 (4/5 v/v) so that the pH of the final suspension is about 2. Then, the analyses by laser diffraction were realized on this diluted suspension. After this “neutralization”, it was verified until several months later that the system does not evolve any more.

On the other hand, on line measurements were done using acoustic spectroscopy. Sound waves interact in a similar manner to light waves but have the advantage that they can travel through concentrated suspensions or emulsions. Ultrasonic attenuation spectroscopy is capable for examining the concentrated or optically opaque systems without any dilution. Such in-situ characterization of concentrated systems makes the acoustic method very useful because it does not need to modify the dispersion state of the suspending particles. Acoustic spectroscopy, as a particle sizing technique, consists in measuring the acoustic attenuation spectrum of a dispersed sample (suspension or emulsion) over a given frequency range. The attenuation of the sound of the suspension provides important information, notably related to the particles size and concentration.

In this work, we had access to the commercial acoustic spectrometer Ultrasizer (Malvern Instruments). Particle size analysis using acoustic spectroscopy consists of:

- Predicting attenuation and velocity spectra by mathematical modelling for any particle size distribution (PSD) and volume concentration,
- Measuring attenuation and velocity spectra,
- Inverting the mathematical model to extract both the PSD and the volume concentration from the measured spectra. Several physical parameters of the suspension are needed to resolve this inverse problem: the densities of the dispersed and continuous phases, the sound speeds, the thermal dilatation coefficients, the thermal conductivities and the heat capacities of the particles and the medium, the shear rigidity of the particles and the viscosity of the medium. This inversion step is mathematically complex and, to simplify the

The Ultrasizer measures the acoustic attenuation spectrum of the sample over the frequency range of 1-150 MHz. The range used for a given measurement depends on the attenuation characteristics of the samples (particle size, solid content). The software of the Ultrasizer is based on the well known ECAH theory (Allegra and Hawley, 1972; Epstein and Carhart, 1953) which predicts that an incidental longitudinal wave interacting with a spherical particle generates compression, thermal and shear waves. The attenuation spectrum of a suspension takes into account the three main types of particle/wave interactions: thermo-elastic, scattering and visco-inertial effects (Dukhin and Goetz, 2001).

The size of the particles suspended in the initial suspension was measured before beginning the aggregation process. By laser diffraction, the mean size is about 80 nm considering a number distribution which is coherent with SEM observations, and about 110 nm for a volume distribution. The size distribution measured by acoustic spectroscopy in terms of volume distribution is less spread and the mean size is around 112 nm. Although they are based on very different physical concepts, laser light diffraction and acoustic spectroscopy give results in a good agreement as it is shown in Fig. 1. It is also important to remember that the analyses performed using the Ultrasizer are in dense conditions (between a few and more than 15 vol. %) whereas they are done in very dilute conditions (about 0.1%) using Mastersizer 2000.

In the case of acoustic spectroscopy, the particle size distributions are basically determined as log-normal law functions. Concerning laser light diffraction, the volume particle size distribution can also be smoothed by a log-normal law. For the volume particle size

distributions of Fig. 1, the properties of the corresponding log-normal laws are reported in Table 1.

Fig. 1

Table 1

*Experimental set-up*

Aggregation experiments were carried out in a standard water jacketed batch agitated vessel of a capacity of 1L. The suspension is stirred with a A310 axial flow impeller (Lightnin). The experimental set-up also includes a thermostatic bath (Fig. 2).

600 mL of a 2 M sodium chloride solution was firstly poured into the tank and put under stirring. When the desired operating temperature was reached, 900 mL of a suspension of colloidal silica at a chosen concentration was added as instantaneously as possible to obtain the desired solid concentration. In such conditions, the final salt concentration was 0.8 M. The suspension was continuously recycled from the stirred batch reactor through the flow cell of the acoustic spectrometer using a peristaltic pump (Masterflex) that allows on-line size analysis. However, the effect of the pump on the aggregates needed to be considered. The main criterion to select the pump and to adjust the flow rate until there was minimum shear on the aggregates. As a result, a peristaltic pump was chosen in preference to other types of pumps. Moreover, the pump was placed downstream of the Ultrasizer, allowing the aggregates to be sampled before passing through the pump.

Fig. 2

**2.2. Following of the PSD**

In this study, the aggregation process was followed in the absence of any other process such as nucleation or particle growth.

*Experimental results*

After different periods of time, samples are removed and in each of them, the aggregation process is stopped using a buffer at pH 2. The samples are then diluted in water in order to get an appropriate dilution for the laser light diffraction analysis. To confirm the results, particle size distributions were also evaluated from acoustic measurements performed on-line of the process without any dilution.

Fig. 3 presents the particle size distributions of samples taken after different periods of time during the aggregation of Klebosol 30R50 silica at 6 % w/w and measured by laser light diffraction.

Fig. 3

At the beginning of the process ($t = 0^+$), the monomodal log-normal curve of the particle size distribution has a mean size of 112 nm. The particles aggregation is clearly illustrated by the shift of the distribution towards the largest sizes. During the first hour, the mean size does not change a lot but the geometric deviation increases (the width of the distribution is increasing). Then an important change in size can be seen as aggregation proceeds once the process time exceeded 60 min: the distribution becomes bimodal. The apparition of the second population is probably due to the formation of quite large aggregates while the first peak moves gradually towards the larger sizes and decreases in intensity. It can be thought that the suspended particles are of two types: a first population of primary particles and small aggregates which evolves slowly and tends to disappear to the benefit of the second population constituted of larger aggregates.

In parallel, the Ultrasizer was used to follow the aggregation on-line of the process as a function of time. Thus, the attenuation spectra were recorded during this experiment each 30 min on a whole period of 8 hours. Some of these spectra are presented on Fig. 4.

Fig. 4

The curve at time t = 0 is the spectrum recorded in the initial suspension before the aggregation begins. At time t = 60 min, the slope of the curve has significantly decreased indicating that the particle dispersion suffered an important destabilization phenomenon by aggregation. At further times, the change in the spectra is still observed resulting from the presence of larger aggregates, but after a certain period, the slope change is less significant indicating that the size of the aggregates did not evolve any more. It can then be supposed that the aggregation process was almost completed within 8 hours. The evolution of the acoustic spectra is quite consistent with the observations done previously about the evolution of the PSD determined by laser diffraction.

In a previous paper (Tourbin and Frances, 2007), it was demonstrated the existence of multiple scattering of acoustic spectroscopy throughout the suspension caused by an overlapping of the viscous and thermal skin surrounding the particles. This phenomenon observed in the case of the Klebosol 30R50 on the whole range of concentration considered in this study is enhanced by the very small size of silica particles. The introduction of a correction factor to the acoustic spectra was recommended to extract correct PSD (Tourbin and Frances, 2007).

Taking into account of the multiple scattering of the ultrasonic wave through the suspension, the particle size distributions of the suspension relating to the destabilization process were then calculated (Tourbin and Frances, 2008). They are reported on Fig. 5. As it can be observed, the aggregation process is again well characterized by the shift of the distributions towards the largest sizes. The evolution of the particle size distribution shows the apparition of a second population of particles after about 120 min of process. However, the peak which corresponds to those large aggregates is determined with a great imprecision. Indeed, the

distribution is sensible to the calculation parameters introduced by the experimenter (fixed or variable input for the calculation of the solid concentration, allowed minimum standard deviation on the particle size distribution, etc.). In this example, the peak of aggregates corresponds to a low volume percentage; therefore it corresponds to a low number of particles that do not contribute enough to the total attenuation. Moreover the introduction of a correction factor to take into account of multiple scattering also probably contributes to the low reliability of the determined particle size distribution. However, the results obtained by both techniques are in good agreement that leads to an important conclusion: silica aggregates are few or not influenced by the dilution step. Since results got by laser diffraction are more precise, the analysis of the evolution of the particle size distributions during the aggregation process and the further numeric study will be made in this study on the base of the laser diffraction results.

Fig. 5

*Aggregation mechanisms*

From these results, it can be supposed that the silica aggregation process is the succession of at least two aggregation stages probably resulting from two distinct mechanisms. It corresponds to what some authors named the two stages of perikinetic aggregation. First, the collisions between primary particles of 80 nm are brought about by a slow perikinetic mechanism for particle sizes smaller than 100 nm leading to a slow increase of the width of the distribution from the primary particle size towards the largest ones. This stage is followed by a rapid mechanism for the coarse particles resulting in the apparition of large aggregates that form a second population of about 1 μm.

This passage of a slow phase of aggregation to a fast one can be explained by the increase of the frequency of the collisions between particles when the aggregates start to grow. In Fig. 6,

the theoretical collision frequency of a particle with a diameter of 100 nm with another particle of diameter ranging from 10 nm to 10 μm is presented when particles motion is caused by diffusion or agitation.

Fig. 6

Thus, the first stage of the aggregation process is relatively slow because the motion of the small particle is brought about by diffusion (Brownian motion). When the suspension begins to be constituted by primary particles and aggregates, the frequency of collision increases and the aggregation becomes faster because the collisions mainly result from the fluid motion (principally by agitation). In this second stage, the collision frequency is higher because the particles overcome easily the potential barrier as a result of their relative motion (Schaer et al., 2001).

## 3. Modelling of the silica aggregation process

Population balance is a highly capable mathematical tool to model the evolution of the properties of the dispersed phases during a process. In the case of our aggregation process, one of the main difficulties for modelling is the choice of the aggregation and breakage kernels. The second difficulty rests with the solving method.

In this work, the Kumar and Ramkrishna (1996) discretized method was used.

The objective of the modelling approach in this study was not to find kinetic models of the aggregation and breakage kernels, but to justify theoretically the experimental observations. For this purpose, different aggregation kernels were tested and the evolution of the calculated PSD were compared to that observed on the experimental part.

### 3.1. The Population Balance Equation (PBE)

According to the works of Smoluchowski (1917), the modelling of the destabilization process can be achieved by the following population balance equation:

$$\frac{\partial n(v,t)}{\partial t} = \frac{1}{2}\int_0^v n(v-v',t)\,n(v',t)\,\beta(v-v',v')\,dv' - \Gamma(v)\,n(v,t) - \int_0^\infty n(v,t)\,n(v',t)\,\beta(v,v')\,dv' + \int_v^\infty \alpha(v,v')\,\Gamma(v')\,n(v',t)\,dv' \quad (1)$$

with $n(v,t)$ the density of particles with size between $v$ and $v+dv$ at $t$, $\beta(v,v')$ the aggregation kernel for a collision between particles of volume $v$ and $v'$, $\Gamma(v)$ the breakage kernel of a particle of size $v$ and $\alpha(v,v')$ the number of « daughter » particles of size between $v$ and $v'$ formed after the breakage of a particle of volume $v'$.

The different terms of the population balance equation are, in order, the term of birth of particles by aggregation, the term of death of particles by breakage, the term of death of particles by aggregation and the term of birth of particles by breakage. (Kumar and Ramkrishna, 1996)

### 3.2. Discretized numeric method

*Discretized population balance equations*

A discretization numerical method was chosen in this work because this method only needs a relatively low computational charge since the complex balance equation is solved like a set of ordinary differential equations. Furthermore, it was demonstrated that it enables to calculate the particle size distributions with a great precision. To solve this equation, the Hounslow et al. (1988) and Kumar and Ramkrishna (1996) methods were used.

By this discretization method, the population balance equation for pure aggregation is

$$\frac{dN_i(t)}{dt} = \sum_{\substack{j,k \\ x_{i-1}\le(x_j=x_k)\le x_{i+1}}}^{j\ge k} \left(1-\frac{1}{2}\delta_{j,k}\right)\eta\beta_{j,k}N_j(t)N_k(t) - N_i(t)\sum_{k=1}^{M}\beta_{i,k}N_k(t) \quad (2)$$

with $$\eta = \begin{cases} \dfrac{x_{i+1}-v}{x_{i+1}-x_i}\ , & x_i \le v \le x_{i+1} \\ \dfrac{x_{i-1}-v}{x_{i-1}-x_i}\ , & x_{i-1} \le v \le x_i \end{cases} \tag{3}$$

and $$\beta_{j,k} = \beta\left(x_j, x_k\right). \tag{4}$$

And for pure breakage, the PBE is

$$\frac{dN_i(t)}{dt} = \sum_{k \ge i} n_{i,k}\Gamma_k N_k(t) - \Gamma_i N_i(t) \tag{5}$$

with $\Gamma_k = \Gamma(x_k)$

and $n_{i,k}$ is the contribution to population at $i$th representative size due to the breakage of a particle of a size $x_k$

$$n_{i,k} = \frac{x_{i+1} - B_{i,k}}{x_{i+1} - x_i} + \frac{x_{i-1} - B_{i-1,k}}{x_i - x_{i-1}} \tag{6}$$

where $$B_{i,k} = \int_{x_i}^{x_{i+1}} v\alpha\left(v, x_k\right)dv \tag{7}$$

The final discrete population balance equation for simultaneous aggregation and breakage is a combination of both previous equations:

$$\frac{dN_i(t)}{dt} = \sum_{\substack{j,k \\ x_{i-1} \le (x_j = x_k) \le x_{i+1}}}^{j \ge k} \left(1 - \frac{1}{2}\delta_{j,k}\right)\eta\beta_{j,k}N_j(t)N_k(t) - N_i(t)\sum_{k=1}^{M}\beta_{i,k}N_k(t) + \sum_{k=i}^{M} n_{i,k}\Gamma_k N_k(t) - \Gamma_i N_i(t) \tag{8}$$

*Preliminary calculations*

The numerical work presented in this study was derived from that of Coufort et al. (2006). The same computational method was used, but the numeric code was modified to suit to our system.

The volume was chosen as the internal coordinate. The volume is discretized following a geometrical progression: $v_{i+1} = s\ v_i$, where $s$ is the experimental ratio of the geometrical progression used in laser diffraction analysis allowing an easier comparison between numerical and experimental results. Thus, all the experimental data in length coordinates were transformed.

The experimental number of class (laser diffraction results) is 99 but for a better precision, the modelling could be realized with a higher number of classes.

Particles of class $k$ could be considered to have a volume $v$ between $v_k$ and $v_{k+1}$. And the set of particles of this class represents a portion of the entire population of particles written:

$$\%(nb)_k = \frac{number\ \ of\ \ particles\, in\ \ the\ \ class}{total\ \ number\ \ of\ \ particles} \tag{9}$$

It was noted that the measured PSD can be well approximated by log-normal distributions,

then $$\%(nb)_k = \int_{v_k}^{v_{k+1}} f(x)dx = \int_{v_k}^{v_{k+1}} \frac{1}{\sqrt{2\pi\sigma^2}} \exp\left(-\frac{(\ln(x)-\mu)^2}{2\sigma^2}\right)\frac{dx}{x} \tag{10}$$

If $$y = \frac{\ln(x)-\mu}{\sqrt{2\sigma^2}} \tag{11}$$

Then $$\int_{v_k}^{v_{k+1}} \frac{1}{\sqrt{2\pi\sigma^2}} \exp\left(-\frac{(\ln(x)-\mu)^2}{2\sigma^2}\right)\frac{dx}{x} = \frac{1}{\sqrt{\pi}} \int_{(\ln(v_k)-\mu)/\sqrt{2\sigma^2}}^{(\ln(v_{k+1})-\mu)/\sqrt{2\sigma^2}} \exp(-y^2)dy \tag{12}$$

And finally $$\%(nb)_k = \frac{1}{2}\left(erf\left(\frac{\ln(v_{k+1})-\mu}{\sqrt{2\sigma^2}}\right) - erf\left(\frac{\ln(v_k)-\mu}{\sqrt{2\sigma^2}}\right)\right) = N_k \tag{13}$$

with $$\mu = \frac{\sum_{k=1}^{nc-1} \ln(v_k) \times \%(nb)_k}{n_c} \tag{14}$$

and $$\sigma = \frac{\sum_{i=1}^{n_c} (\ln(v_k)-\mu)^2 \times \%(nb)_k}{n_c - 1} \tag{15}$$

respectively the geometric mean size and the standard deviation of the distribution. “erf”, is the notation of the error function.

Since the experimental results are presented on a mass basis, the last modification is the transformation of the number percentages (determined by the computation) in mass percentages. The mass fraction of particles in the $[v_{i-1};v_i]$ volume range is

$$w_i = \frac{\Delta M_i}{M_0} \tag{16}$$

with $M_0$ the total mass of particles and $M_i$ the mass of particles in the $[L_{i-1};L_i]$ experimental length range.

And for each class, the number of particles is

$$N_i = \frac{M_i}{\rho_p v_i} = \frac{[SiO_2]_i}{\rho_p v_i} M_0 = \frac{w_i [SiO_2]}{\rho_p v_i} V_t \tag{17}$$

where $\rho_p$ is the silica particles density *($\rho_p$= 2369 kg/m$^3$)*, *[$S_iO_2$]* is the silica total mass concentration *(kg.m$^{-3}$)* and $V_t$ the total volume of the suspension *($V_t$=1.5 L)*.

### 3.3. Validation of the model

In this code, the temporal integration of the system of differential equations is done by Matlab® ode23s function.

The code was validated using a log-normal law for the initial particle size distribution in accordance with the experimental observations.

Lee et al. (1997) gave an analytical solution of the population balance in case of a brownian kernel of that kind:

$$\beta = \beta_0 \left(u^{1/3} + v^{1/3}\right)\left(\frac{1}{u^{1/3}} + \frac{1}{v^{1/3}}\right). \tag{18}$$

Then, the analytical solution of the population balance (pure aggregation) is:

$$N(t) = \frac{N_0}{1 + A\beta_0 N_0 t} \tag{19}$$

with $N_0$ the total number of initial particles, $A=1+exp(Z_0)$ with $Z_0=ln^2(\sigma_0)$ and $\beta_0=2k_BT/3\eta$. $\sigma_0$ is the geometric standard deviation of the initial distribution.

The experimental initial distribution was obtained by smoothing the experimental points for the following operating conditions *[Si0$_2$]= 10% / [NaCl]= 0.8M / T=298K / r=450 rpm.* Moreover, $T=298\ K$ and $\eta=1.13\ 10^{-3}\ Po$, giving an approximation of $\beta_0$ equal to $2.44\ 10^{-18} m^3.s^{-1}$.

For $|\beta_0| \approx 2.44\ 10^{-18}$, the numerical and analytical solutions of the evolution of $N(t)/N_0$ were compared (Fig. 7).

It can be observed that the calculated total number of particles varies similarly to the total number determined by the analytical solution but it remains always lower. The difference between both functions increases with time because larger the particles are, more the number particles density decreases quickly (exponential trend).

If the number of discretized classes increases, the resolution is better and the difference

$$\left(\frac{N_{numerical}(t)}{N_0}\right)^2 - \left(\frac{N_{analytical}(t)}{N_0}\right)^2 \qquad (20)$$

is about 6% for *100 classes* and 2% for *200 classes*.

Then, it can be concluded that the model accurately predicts the decrease of the number of particles during the aggregation with a size dependent kernel (then, all the more, in case of size independent kernel).

Fig. 7

### 3.4. Aggregation mechanisms

*Single aggregation kernel*

First, it was tried to model the aggregation process by a single mechanism of collision, the term of breakage being set to zero.

A constant kernel ( $\beta(u,v) = \beta_0$ ) characterizes the collisions between particles of the same size in brownian motion. The value of $|\beta_0|$ = 6.9x10$^{-15}$ ($\beta_{0,b}=2k_BT/3\eta$ calculated in m$^3$.h$^{-1}$; this value corresponds to the previous one: *2.44 10$^{-18}$m$^3$.s$^{-1}$*) was chosen on the base of the experimental data. The evolution during time of the silica volume concentration distributions calculated by the model, versus the volume of particles is represented on Fig. 8. The formation of aggregates is observed. The PSD remains monomodal, with a mean size that evolves gradually towards the larger sizes and a low dispersion around.

The evolution of the PSD is on the same type for a Brownian kernel (Smoluchowski, 1917) ( $\beta(u,v) = \beta_{0,b}(u+v)\left(\frac{1}{u}+\frac{1}{v}\right)$ ) that characterizes the collisions between particles of different sizes by Brownian motion (Fig. 9).

This type of evolution is very different to those observed experimentally that proves that a constant or a Brownian kernel is not convenient to model the processes observed experimentally.

To take a better account of the hydrodynamics of the stirred tank, a sum kernel (Camp and Stein, 1943; Smit et al., 1994; Smoluchowski, 1917) ( $\beta(u,v) = \beta_{0,s}(u+v)$ ) which characterizes the orthokinetic collisions between particles in a laminar or a turbulent flux was tested. By estimation of the value of the shear gradient in the stirred tank *($\beta_0$=G=$\sqrt{(\varepsilon/\nu)}$* the value of *$|\beta_0|$ = 1.1 10$^{-19}$* was chosen, taking hours and nanometers as reference units for the calculation. As it can be seen on Fig. 10, larger aggregates than previously are formed but the PSD remain monomodal once again.

Fig. 8

Fig. 9

Fig. 10

None of those kernels characterize well the mechanisms that lead to the aggregation of colloidal silica suspensions in a stirred tank since they are unable to describe a bimodal distribution. It is clear that the process involved are more complex and need to be modelled in a more complex way.

*Multiple aggregation kernels*

From the experiments, it was suspected that there were at least two aggregation mechanisms with different kinetics. A first one, governed by the physico-chemical parameters of the system and a faster one submitted to the hydrodynamic conditions (Tourbin and Frances, to be published). Futhermore, some remarkable particle sizes can be extracted from the experimental results: the particle size that separates the two granulometric peaks (Fig. 3) or the maximal aggregate size. Similar observations were done by Schaer (1997) and David et al. (2003).

In the present study, the experiments conduced us to introduce two characteristic sizes for the aggregation process: $V_j$, the "junction" size between the two peaks and $\lambda_k$, the Kolmogorov micro-scale of the agitated system. According to the operating conditions, the two types of aggregation may occur: Brownian aggregation and laminar or turbulent aggregation. The possibility of the occurrence of both mechanisms successively was considered in the way:

- for two particles of volume $v_i$ and $v_j$ colliding together, if $v_i<V_j$ and $v_j<V_j$, the brownian aggregation kernel (which quantifies the efficiency of the collisions) was used:

$$\beta_b\left(v_i, v_j\right) = \beta_{0,b}\left(v_i + v_j\right)\left(\frac{1}{v_i} + \frac{1}{v_j}\right) \tag{21}$$

- and if at least one of the volume is higher than $V_j$ ($v_i<V_j$ and $v_j>V_j$ or $v_i>V_j$ and $v_j>V_j$), the sum kernel was used:

$$\boldsymbol{\beta}\left(\boldsymbol{v_i}, \boldsymbol{v_j}\right) = \boldsymbol{\beta}_{0,s}\left(\boldsymbol{v_i^3} + \boldsymbol{v_j^3}\right) \tag{22}$$

Alternatively, the second form of the sum kernel currently used for laminar regime and isotropic turbulence could be used:

$$\beta(v_i, v_j) = \beta_{0,s}(v_i + v_j)^3 \tag{23}$$

An optimization code based on the Simplex method (Porte, 2002) was added in order to minimize the discrepancy between the experimental and the numeric curves. The objective values of the subroutine were the aggregation kernels, $\beta_{0,b}$ (Brownian kernel) and $\beta_{0,s}$ (sum kernel), and $V_j$.

Here is the validation realized for two different experiments. The initial values are the same as previously: $|\beta_{0,b}|=6.9\ 10^{-15}$ and $|\beta_{0,s}|=1.1\ 10^{-19}$.

The first test corresponds to the following experimental operating conditions: *[Si0$_2$]= 10% / [NaCl]= 0.8M / T=298K / r=450 rpm.* Moreover, $\eta=1.13\ 10^{-3}$ *Po*.

On Fig. 11, the PSD calculated by the model are reported. The best fit was obtained using eq.(22) for the sum kernel. The optimized vector [$\beta_{0,b}$ , $\beta_{0,s}$ , $V_j$] is equal to [$4.46\ 10^{-24}$, $6.61\ 10^{-20}$, 12743] and the optimization error calculated by the mean square method,

$$\sum_i \left(N_i^{num}(t)\right)^2 - \left(N_i^{\exp}(t)\right)^2 \tag{24}$$

is equal to 7.15.

Fig. 11

By this way, the real aggregation mechanisms are better represented. Indeed, using the two different aggregation kernels, first the Brownian one representative of the collisions between the primary particles and between the primary particles and the small aggregates, and then a second one representative of the collisions between larger aggregates, two populations of

particles are finally noticed on the modelled PSD. The peak of primary particles decreases in intensity but the value of $\beta_{0,b}$ is high enough to allow the moving of the peak to move towards the larger sizes. Furthermore, from the volume $V_j$, the use of the sum kernel allows the increase and the move of the second peak whose evolution is not exactly what was observed experimentally. At last, the final sizes of each population, and more particularly of the population of larger aggregates, are of the same order of magnitude than the sizes measured at the end of the experiments.

Another set of operating conditions was tested with the modelling code: *[$Si0_2$]= 20% / [NaCl]= 0.8M / T=338K / r=450 tr.min$^{-1}$*. For those conditions, the values of the constant of the aggregation kernels are different because they take into account the physico-chemical and hydrodynamic conditions of the system. Then, for this case, the initialization values were $[\beta_{0,b}\ ,\ \beta_{0,s}\ ,\ V_j] = [1.9\ 10^{-18},\ 1.1\ 10^{-19}\ ,\ 10^4]$. The results are represented on Fig. 12. The optimized values are $[\beta_{0,b},\ \beta_{0,s}\ ,\ V_j] = [1.63\ 10^{-18},\ 6.23\ 10^{-20},\ 2\ 10^3]$ and the optimization error is equal to 15.99. It can be noted that a higher temperature than previously investigated implies a higher value of the Brownian kernel constant, and then reflects on a faster appearance of the second population and a more numerous population of large aggregates. As it can be seen, the use of two successive aggregation kernels again correctly represents the aggregation mechanisms that occurred in the experimental system.

Fig. 12

On Fig. 13, in order to compare the experimental and modelled PSD, both of them are represented in case of the first set of operating conditions. As discussed previously, it can be observed that those results are really promising. The fit can not be perfect principally because of the fact that the experimental analytical technique allows the widening of the peak and a

"creation" of smaller particles, which is not physically acceptable (no fragmentation of primary particles neither nucleation are possible).

Fig. 13

Those two examples of results obtained by the model underline the necessity to use several kernels, that are characteristic of the existence of at least two different mechanisms during the aggregation process, and that justifies the existence of two populations of particles.

In the last part, it would be taken into account of the breakage process which is in competition with the aggregation one and leads to the real final size of particles in the agitated tank.

*Coupled aggregation and breakage*

The breakage terms (equations of apparition and disappearance, breakage kernel and function of repartition) are now considered in the equations solver.

It is considered that when a particle of size *v'* breaks, it gives two particles of volume *v*. Then, the number of particles of volume between *v* and *v+dv* formed by the rupture of a particle of volume *v'* is defined by

$$\alpha(v,v') = 2/v' \tag{25}$$

Two different forms of the breakage kernel were analyzed: a power law function as used by Hounslow et al. (1988) and Kumar and Ramkrishna (1996)

$$\Gamma(v) = \Gamma_0 v^x \tag{26}$$

and an exponential breakage kernel :

$$\Gamma(\boldsymbol{v}) = \Gamma_0 \boldsymbol{e}^{x\boldsymbol{v}} \tag{27}$$

For first approximation, it was chosen to take $\Gamma_0 = 1$. A better agreement was finally obtained using the power law function for the breakage kernel. Fig. 14, 15 and 16, represent

the results of modelling of the aggregation of silica particles for the first operating conditions with $[\beta_{0,b}\ ,\ \beta_{0,s}\ ,\ V_j] = [10^{-22},\ 10^{-18},\ 10^{5}]$ (values closed to the optimized values of the previous modelling) and with $x$ respectively equal to $10^{-1}$, $10^{-2}$ and $5.10^{-2}$.

Fig. 14

Fig. 15

Fig. 16

It can be observed that for $x=10^{-1}$, the breakage is too important because at the end of the process, only one population is observed and all the particles are too small. On the contrary, the breakage is not enough when $x=10^{-2}$ because the size of the aggregates is too large and the speed of appearance of larger aggregates is too important. But, in this case, two populations are observed. Finally, an intermediate value $(x=5.10^{-2})$ looks better to approximate the experimental results. Two populations of particles were observed and the order of magnitude of sizes was quite good (about 130 nm for the first peak and about 10 µm for the second one). Of course, there is still a noticeable discrepancy between the experimental and the calculated size distributions. It must be remembered that this work was based on the assumption that each collision leads to the formation of an aggregate, which corresponds to collision efficiencies all equal to one. But it was demonstrated (Elimelech et al., 1995; Han and Lawler, 1992) that, depending on the physicochemical and hydrodynamic properties of the system, the collision efficiency is usually lower than one.

Furthermore, many other simplifications were introduced into the model: the particle morphological variability was not taken into account, a strong simplification was done on the breakage mechanism (two particles of volume $v$ are produced when a particle of volume $v'$ is broken), the initial experimental data were fitted by a log-normal law, the aggregation mechanisms were assumed successive with a unique and fixed pivot volume $V_j$, only a mean

shear gradient was considered in turbulent flow regime, etc. . However, despite of these simplifications, the trend of the particle size distributions versus the aggregation process are well reproduced by the model confirming the hypothesis of two successive aggregation mechanisms coupled with the breakage of the largest aggregates.

## 4. Conclusion

In this paper, an experimental and a numerical study of the aggregation of dense colloidal silica suspension in a stirred tank were developed. The experimental hypothesis of a complex coupling between aggregation and breakage processes was confirmed by the numeric approach based on the discretized Kumar and Ramkrishna (1996) solving method of population balance.

Indeed, it was proved that the aggregation of colloidal silica does not result of a single mechanism but it is the combination between at least two different aggregation processes and breakage according to the operating conditions.

The use of the two different aggregation kernels confirms the existence of:

- a first aggregation phase between primary particles where the collisions are due to the brownian motion of the particles (slow perikinetic aggregation)
- and then a second phase where the collisions are due to the particles motion carried along by the fluid motion. Those collisions of aggregates between them lead to very large aggregates (fast perikinetic aggregation while the aggregates size is lower than the Kolmogorov micro-scale).

By modelling, thereby the collision rates were determined. The values of the brownian diffusion constant ($\beta_0=2k_BT/3\eta$) and of the shear gradient ($\beta_0=G/6=1/6*\sqrt{(\varepsilon/\nu)}$) are in agreement with the experimental results.

**5. Acknowledgements**

The authors gratefully acknowledge Pr A.Liné and Dr C. Coufort from the LISBP (INSA, Toulouse) who gave the code from which the work on modelling presented in this study is derived.

**6. Nomenclature**

| | |
|---|---|
| $G$ | Shear gradient ($s^{-1}$) |
| $k_B$ | Blotzmann constant *($k_B=1.381.\ 10^{-23}$ J.K-1)* |
| $L$ | Size (length) of the particle (m) |
| $L_0$ | Minimal size of the particle (m) |
| $L_{ar}$ | maximal size observed by Schaer (1997) during the slow perikinetic aggregation |
| $M_i$ | Mass of particles in the $[L_{i-1},L_i]$ range (kg) |
| $M_0$ | Total mass of particles (kg) |
| $n(v,t)dv$ | Number of particles of size between $v$ and $v$+dv at time $t$ (-) |
| $n_c$ | Number of size classes (-) |
| $n_{i,k}$ | Number of particles produced at the pivot $x_i$ from the breakage of an aggregate of size $x_k$ (-) |
| $N_i(t)$ | Number of particles in class $i$ at $t$ (-) |
| $N(t)$ | Total number of particles at $t$ (-) |
| $N_0$ | Total number of particles at $t=0$ (-) |
| $r$ | Speed rate ($s^{-1}$) |
| $s$ | Ratio of the geometric progression used for the discretization (-) |
| $t$ | Time (s) |
| $T$ | Temperature (K) |
| $v$ | Volume of the particle ($m^3$) |

| | |
|---|---|
| $V_j$ | « Junction » size between the two peaks of the PSD ($m^3$) |
| $V_t$ | Total volume of the suspension ($m^3$) |
| $w$ | Mass solid fraction (%) |
| $x_i$ | Representative volume of the class $i$ ($m^3$) |
| $\%(nb)_k$ | Percentage of particles in class $k$ (%) |
| $[SiO_2]$ | Silica mass concentration ($kg.m^{-3}$) |

*Greek Letters*

| | |
|---|---|
| $\alpha(v,v')$ | Number of « daughter » particles of size between $v$ and $v'$ formed after the breakage of a particle of volume $v'$ (-) |
| $\beta(v,v')$ | Aggregation kernel – Collision rate between particles of size $v$ and $v'$ ($m^3.s^{-1}$) |
| $\beta_0$ | Norm of the aggregation kernel (-) |
| $\beta_{0,b}$ | Norm of the brownian aggregation kernel (-) |
| $\beta_{0,s}$ | Norm of the sum aggregation kernel (-) |
| $\varepsilon$ | Turbulent kinetic energy dissipation rate ($m^2.s^{-3}$) |
| $\Lambda$ | Conductivity (S) |
| $\Gamma(v)$ | Breakage frequency of a particle of size $v$ ( $s^{-1}$) |
| $\Gamma_0$ | Norm of the breakage kernel (-) |
| $\lambda_k$ | Kolmogorov Micro-scale (m) |
| $\upsilon$ | Kinematic viscosity ($m^2.s^{-1}$) |
| $\rho$ | Density ($kg.m^{-3}$) |
| $\mu$ | Geometric mean of the PSD ($m^3$) |
| $\sigma$ | Standard deviation (-) |
| $\eta$ | Viscosity (Po) |

*Suscripts*

| | |
|---|---|
| $_b$ | Brownian |
| $_i$ | make reference to the particle *i* |
| $_s$ | Sum |

*Acronym:*

| | |
|---|---|
| PSD | Particle size distribution |

## 7. References


Allegra, J.R., Hawley, S.A., (1972). Attenuation of Sound in Suspensions and Emulsions: Theory and Experiments, Journal of Acoustic Society of America, 51 (5 part 2), 1545 – 1564.

Brakalov L.B., (1987). A connection between the orthokinetic coagulation capture efficiency of aggregates and their maximum size, Chemical Engineering Science, 42 (10), 2373-2383.

Camp, T.R., Stein, P.C., (1943). Velocity gradients and internal work in fluid motion, Journal of Boston Society Civ. Eng., 30, 219-237.

Coufort, C., Bouyer, D., Liné, A., Haut, B., (2006). Modelling of flocculation using population balance equation, Chemical Engineering and Processing, 46(12), 1264-1273.

David, R., Paulaime, A.M., Espitalier, F., Rouleau, L., (2003). Modelling of multiple-mechanism agglomeration in a crystallization process, Powder Technology, 130 (1-3), 338-344.

Dukhin A.S., Goetz P.J., (2001). New developments in acoustic and electroacoustic spectroscopy for characterizing concentrated dispersions, Colloids and Surfaces A: Physicochemical and Engineering Aspects, 192, 267–306.

Elimelech M, Gregory J., Jia X., Williams R.A., (1995). Particle Deposition and Aggregation – Measurement, Modelling and Simulation, Colloid and surface Engineering Series, Butterworth-Heinemann.

Epstein, P.S., Carhart, R.R., (1953). The absorption of sound in suspensions and emulsions. I. Water fog in air, Journal of Acoustic Society of America, 25, 553–565.

Gruy, F., (2001). Formation of Small Silica Aggregates by Turbulent Aggregation, Journal of Colloid and Interface Science, 237 (1), 28-39.

Han M.Y., Lawler D.F., (1992). The (relative) insignificance of G in flocculation, Journal of American Water Works Association, 84, 867-874.

Hounslow, M.J., Ryall, R.J., Marshall, V.R., (1988). A Discretized Population Balance for Nucleation, Growth, and Aggregation, AIChE Journal, 34 (11), 1821-1832.

Israelachvili, J. (1992). Intermolecular and Surface Forces, 2nde edition, Academic Press, Londres.

Kumar, S., Ramkrishna, D., (1996). On the solution of population balance equations by discretization – I. A fixed pivot technique, Chemical Engineering Science, 51(8), 1311-1332.

Kusters K.A., Wijers J.G., Thoenes D., (1991). Aggregation kinetics of small particles in agitated vessels, Chemical Engineering Science, 52 (1), 107-121.

Lee, K.W., Lee, Y.J., Han, D.S., (1997). The Log-Normal Size Distribution Theory for Brownian Coagulation in the Low Knudsen Number Regime, Journal of Colloid and Interface Science, 188, 486-492.

Motoyoshi, M., Skarba, M., Galletto, P., Cakara, D., Borkovec, M., (2005). Effects of heat treatment on the aggregation and charging of Stöber-type silica, Journal of Colloid and Interface Science, 292 (1), 139-147.

Porte, C., (2002). Méthodes directes d'optimisation – Méthodes à une variable et Simplex, Techniques de l'Ingénieur, P 228, 1-18, Editions T.I. Sciences et Techniques.

Schaer, E., (1997). Conception d'un procédé pour la production de microparticules filtrables et redispersables, Thèse de Doctorat, Institut National Polytechnique de Lorraine.

Schaer, E., Ravetti R. and Plasari E., (2001). Study of silica particle aggregation in a batch agitated vessel, Chemical Engineering and Processing, 40 (3), 277-293.

Schantz Zackrisson, A., Martinelli, A., Matic, A., Bergenholtz, J., (2006). Concentration effects on irreversible colloid cluster aggregation and gelation of silica dispersions, Journal of Colloid and Interface Science, 301 (1), 137-144.

Smit, D.J., Hounslow, M.J., Paterson, W.R., (1994). Aggregation and gelation I: Analytical solutions for CST and bach operations, Chemical Engineering Science, 49 (18), 1025-1035.

Smoluchowski, M., (1917). Versuch einer mathematischen Theorie der Koagulationskinetik Kolloider Lösungen, Zeitschrift für physikalische Chemie, 92, 129-168.

Tourbin, M., Frances, C., (2007). A Survey of Complementary Methods for the Characterization of Dense colloidal Silica, Particle and Particle System Characterization, 24(6), 411-423.

Tourbin, M., Frances, C., (2008). Monitoring of the Aggregation Process of Dense Colloidal Silica Suspensions in a Stirred Tank by Acoustic Spectroscopy, Powder Technology, In Press.

Trompette, J.L., Meireles, M., (2003). Ion-specific effect on the gelation kinetics of concentrated colloidal silica suspensions, Journal of Colloid and Interface Science, 263 (2), 522-527.

Wyss, H.M., Innerlohinger, J., Meier, L.P., Gauckler, L.J., Glatter, O., (2004). Small-angle static light scattering of concentrated silica suspensions during in situ destabilization, Journal of Colloid and Interface Science, 271 (2), 388-399.

**Captions of illustrations**

Fig. 1: Comparison of Volume and Number frequency distribution measured by laser diffraction (diluted conditions) and acoustic spectroscopy (suspension solid content = 10 % wt.)

Fig. 2: Experimental set-up

Fig. 3: Particle size distribution measured by laser diffraction. Diluted suspensions of samples taken during the aggregation process. [SiO2] = 6% wt. / [NaCl] = 0.8 M / T = 298 K / stirring speed = 450 rpm.

Fig. 4: Attenuation spectra measured by acoustic spectroscopy in dense conditions on-line of the aggregation process. [SiO2] = 6% w/w / [NaCl] = 0.8 M / T = 298 K / stirring speed = 450 rpm.

Fig. 5: Particle size distribution measured by acoustic spectroscopy in dense conditions on-line of the aggregation process. [SiO2] = 6% w/w / [NaCl] = 0.8 M / T=298 K / stirring speed = 450 rpm.

Fig. 6: Collision frequency for collisions between a particle of a diameter of rj=100 nm and an other particle of diameter of 10 nm<ri<10μm. T=298 K/stirring speed=450 rpm

Fig. 7: Comparison between the analytical and the numerical solutions of the population balance for a brownian aggregation kernel in the case of a log-normal initial distribution (nc=100 classes).

Fig. 8: Simulated evolution of the particle size distributions with a constant kernel $|\beta|=|\beta_0|=2k_BT/3\eta = 6.9x10^{-15}$.

Fig. 9: Simulated evolution of the PSD for a brownian kernel $|\beta_0|=1.1\ 10^{-19}$.

Fig. 10: Simulated evolution of the PSD for a sum kernel $|\beta_0|=1.1\ 10^{-19}$.

Fig. 11: Simulation of the evolution of the PSD using brownian and sum kernels. $[\beta_{0,b}, \beta_{0,s}, V_j]=[\ 4.4\ 10^{-24}, 6.6\ 10^{-20}, 1.27\ 10^{4}]$.

Fig. 12: Simulation of the evolution of the PSD using brownian and sum kernels. [$\beta_{0,b}$ , $\beta_{0,s}$, $V_j$]=[ $1.63\ 10^{-18}$, $6.23\ 10^{-19}$, $2\ 10^{3}$].

Fig. 13: Simulation of the evolution of the PSD using brownian and sum kernels. [$\beta_{0,b}$ , $\beta_{0,s}$, $V_j$]=[ $4.4\ 10^{-24}$ , $6.6\ 10^{-20}$ , $1.27\ 10^{4}$]. Comparison with the experimental results.

Fig. 14: Simulation of the evolution of the PSD for coupled aggregation and breakage. [$\beta_{0,b}$ , $\beta_{0,s}$ , $V_j$] = [$10^{-22}$, $10^{-18}$, $10^{5}$] and x=$10^{-1}$.

Fig. 15: Simulation of the evolution of the PSD for coupled aggregation and breakage. [$\beta_{0,b}$ , $\beta_{0,s}$ , $V_j$] = [$10^{-22}$, $10^{-18}$, $10^{5}$] and x=$10^{-2}$.

Fig. 16: Simulation of the evolution of the PSD for coupled aggregation and breakage. [$\beta_{0,b}$ , $\beta_{0,s}$ , $V_j$] = [$10^{-22}$, $10^{-18}$, $10^{5}$] and x=$5.10^{-2}$.

**Captions of tables**

Table 1: Geometric mean size and standard deviation of the log-normal laws for acoustic spectroscopy particle size distribution and for the smoothing of the laser light diffraction volume distribution.

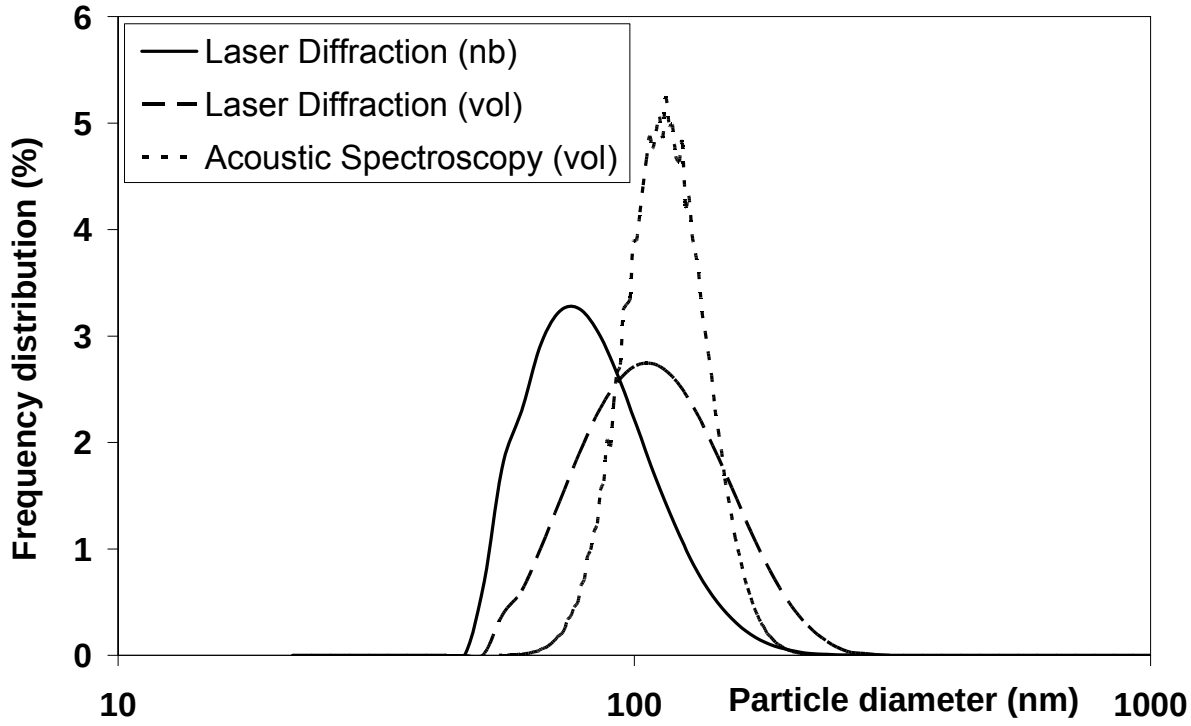
Laser Diffraction (nb)
Laser Diffraction (vol)
Acoustic Spectroscopy (vol)
Frequency distribution (%)
0
1
2
3
4
5
6
10
100
1000
Particle diameter (nm)

**Fig.1**

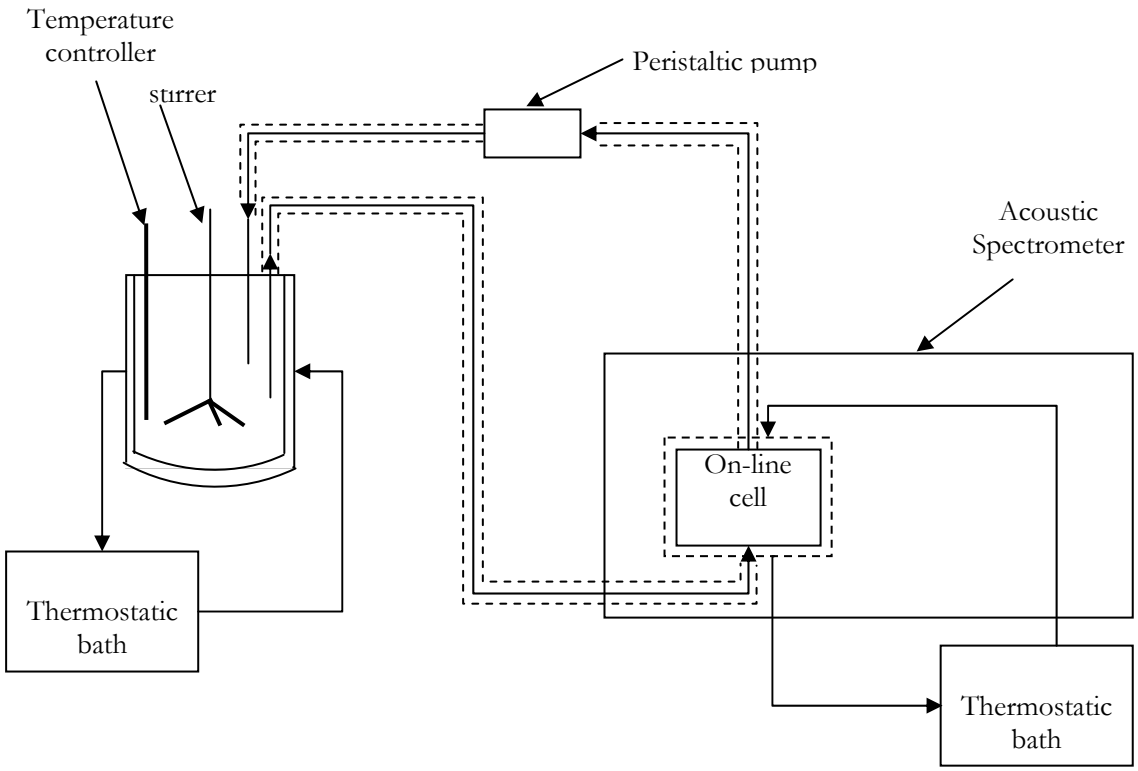
Temperature
controller
stirrer
Peristaltic pump
Acoustic
Spectrometer
On-line
cell
Thermostatic
bath
Thermostatic
bath

**Fig. 2**

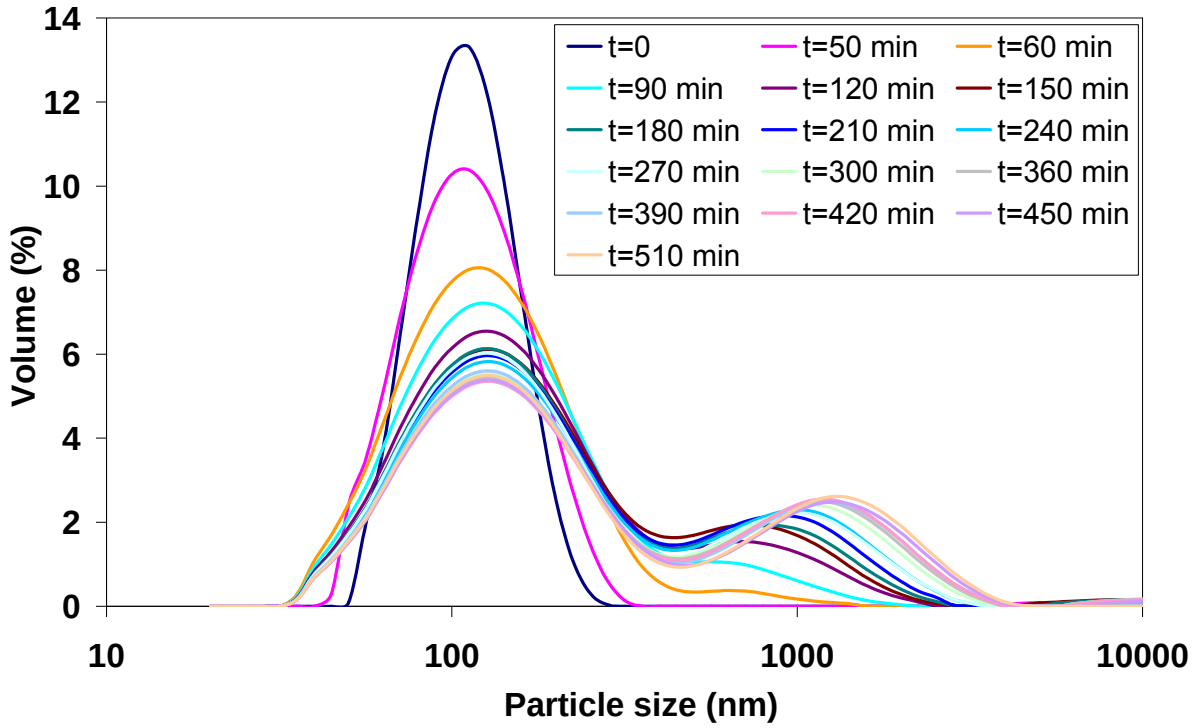
14
12
10
8
6
4
2
0
Volume (%)
10
100
1000
10000
Particle size (nm)
t=0
t=50 min
t=60 min
t=90 min
t=120 min
t=150 min
t=180 min
t=210 min
t=240 min
t=270 min
t=300 min
t=360 min
t=390 min
t=420 min
t=450 min
t=510 min

**Fig.3**

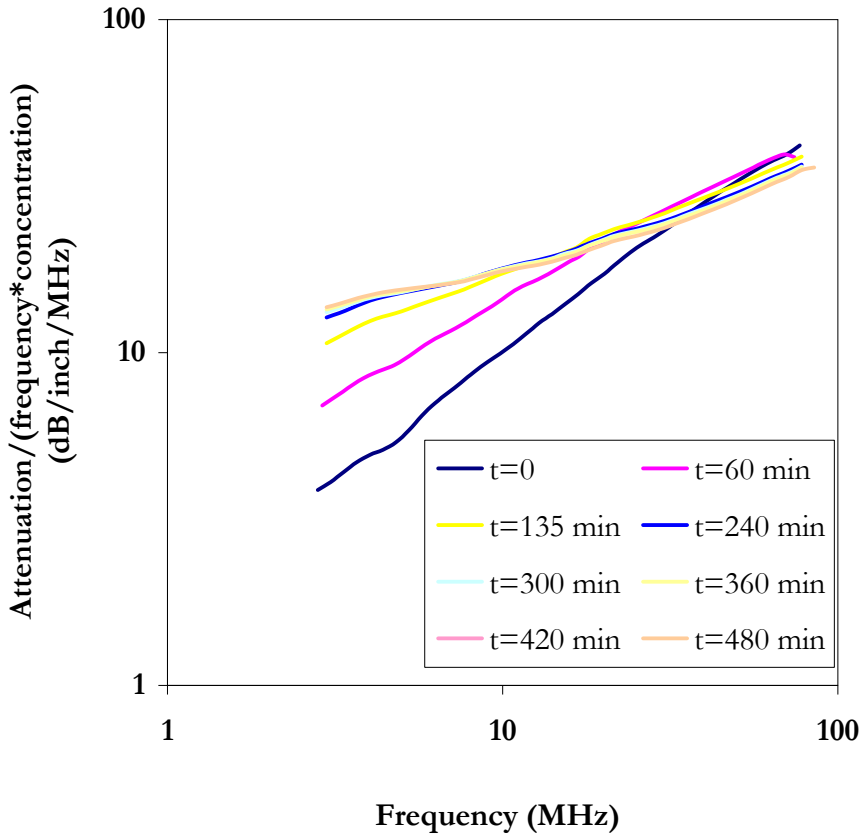
100
10
1
1
10
100
Attenuation/(frequency*concentration)
(dB/inch/MHz)
Frequency (MHz)
t=0
t=60 min
t=135 min
t=240 min
t=300 min
t=360 min
t=420 min
t=480 min

**Fig.4**

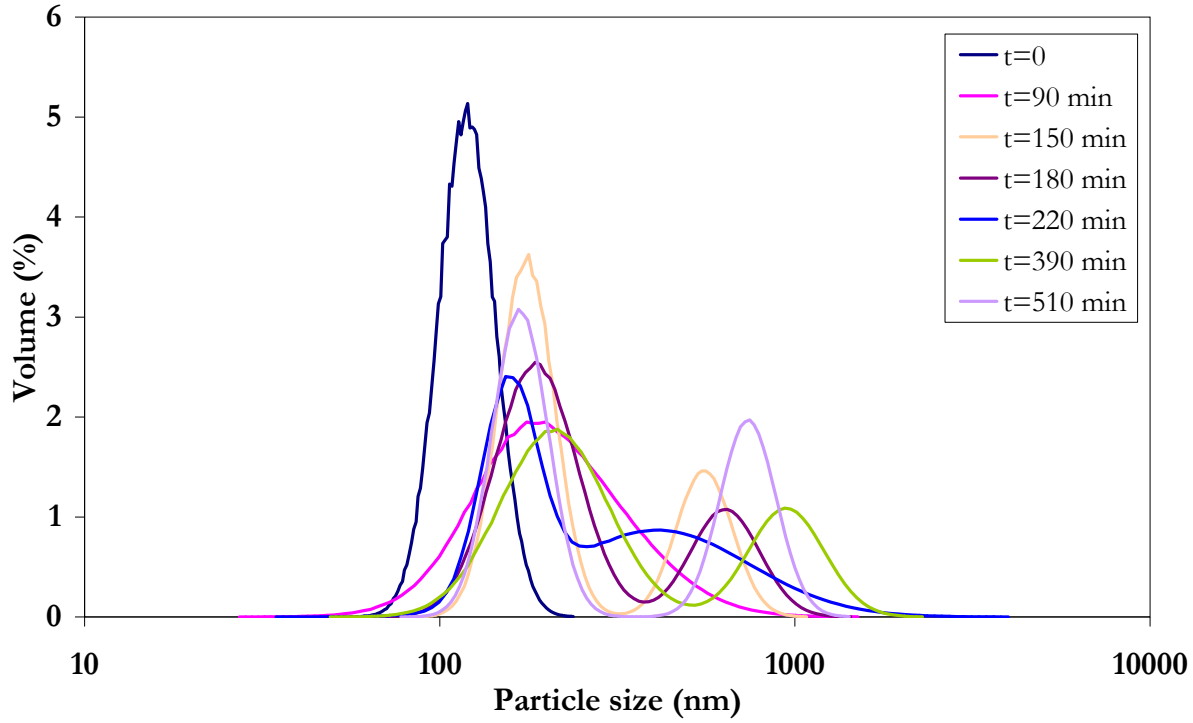
6
5
4
3
2
1
0
Volume (%)
10
100
1000
10000
Particle size (nm)
t=0
t=90 min
t=150 min
t=180 min
t=220 min
t=390 min
t=510 min

**Fig.5**

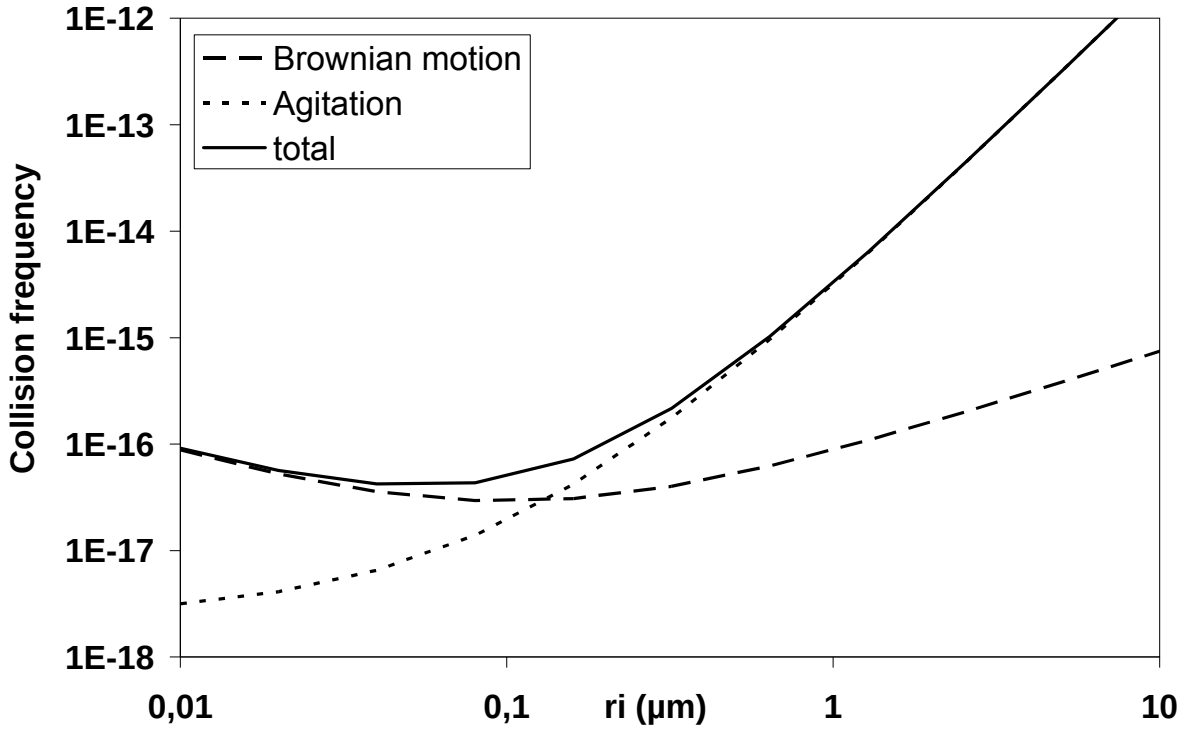
1E-12
1E-13
1E-14
1E-15
1E-16
1E-17
1E-18
Collision frequency
Brownian motion
Agitation
total
0,01
0,1
ri (µm)
1
10

**Fig.6**

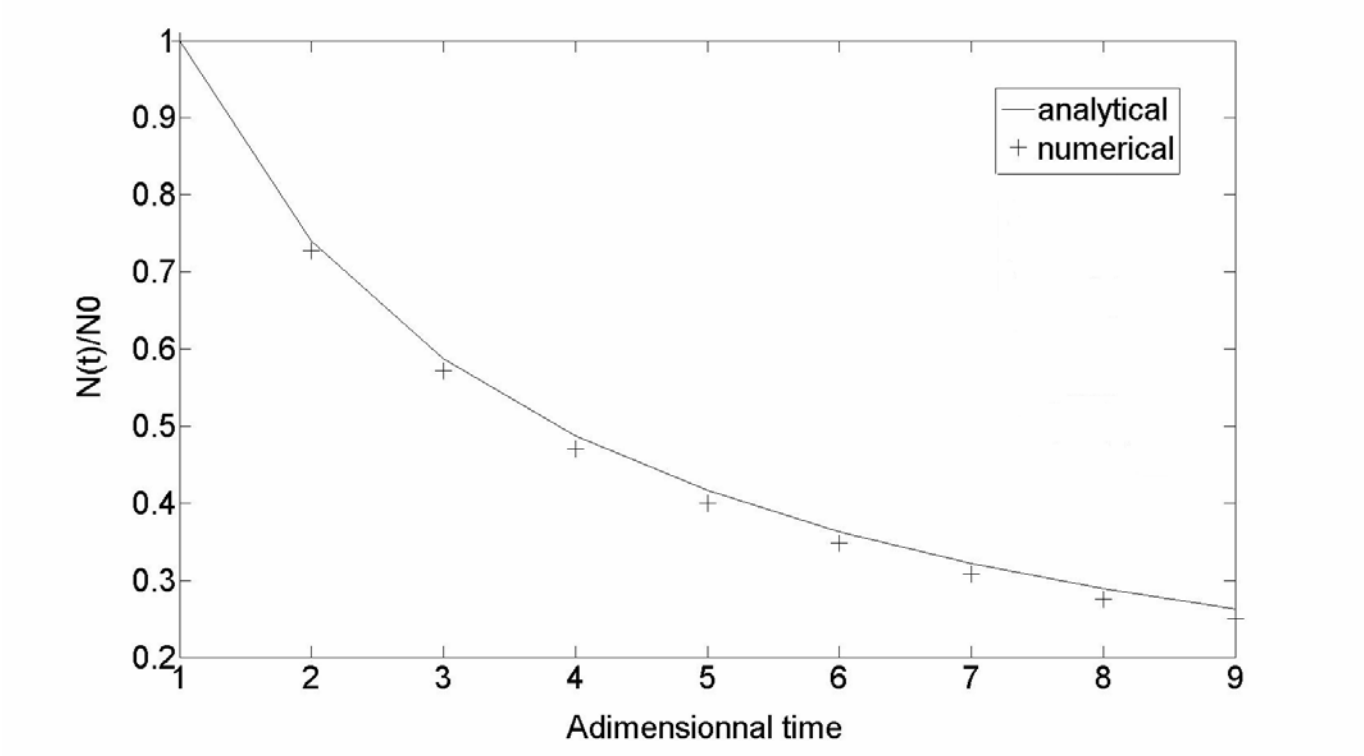
analytical
numerical
N(t)/N0
Adimensionnal time
1
0.9
0.8
0.7
0.6
0.5
0.4
0.3
0.2
1
2
3
4
5
6
7
8
9

**Fig.7**

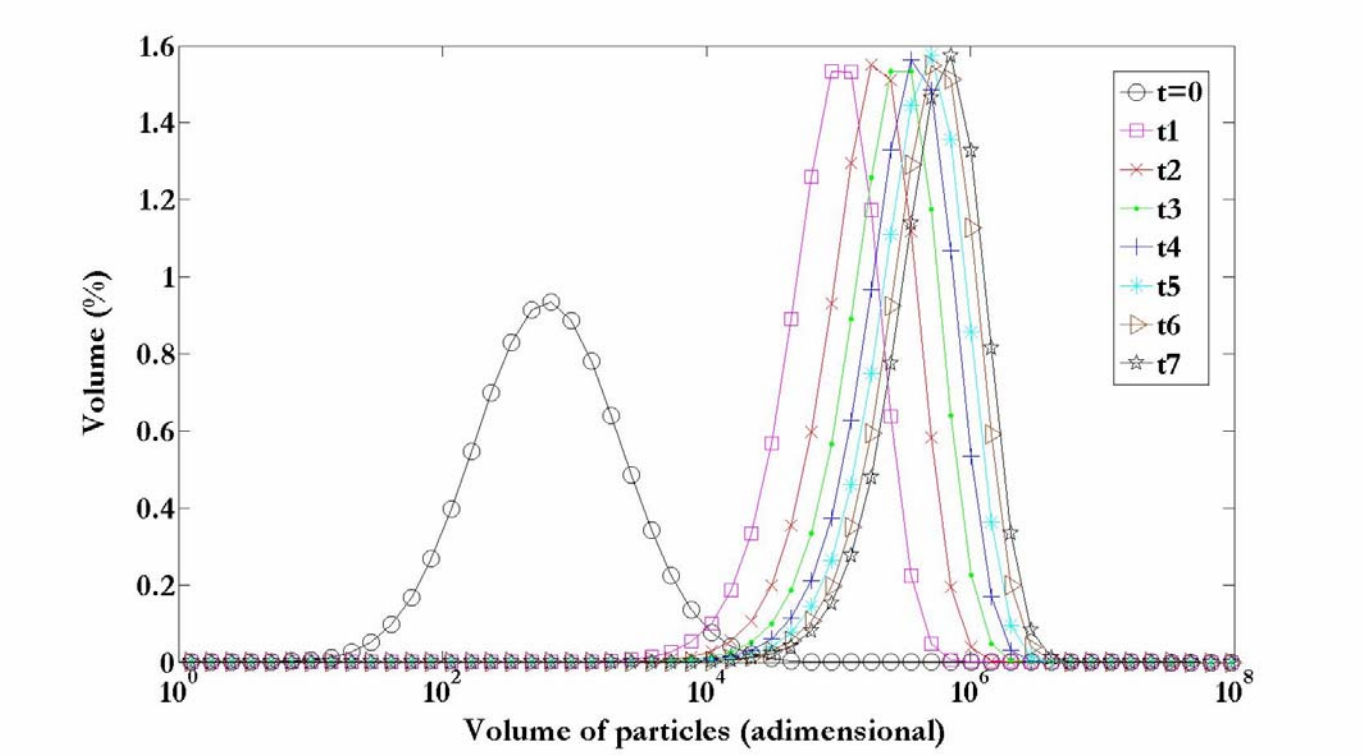
Volume (%)
Volume of particles (adimensional)
t=0
t1
t2
t3
t4
t5
t6
t7

**Fig.8**

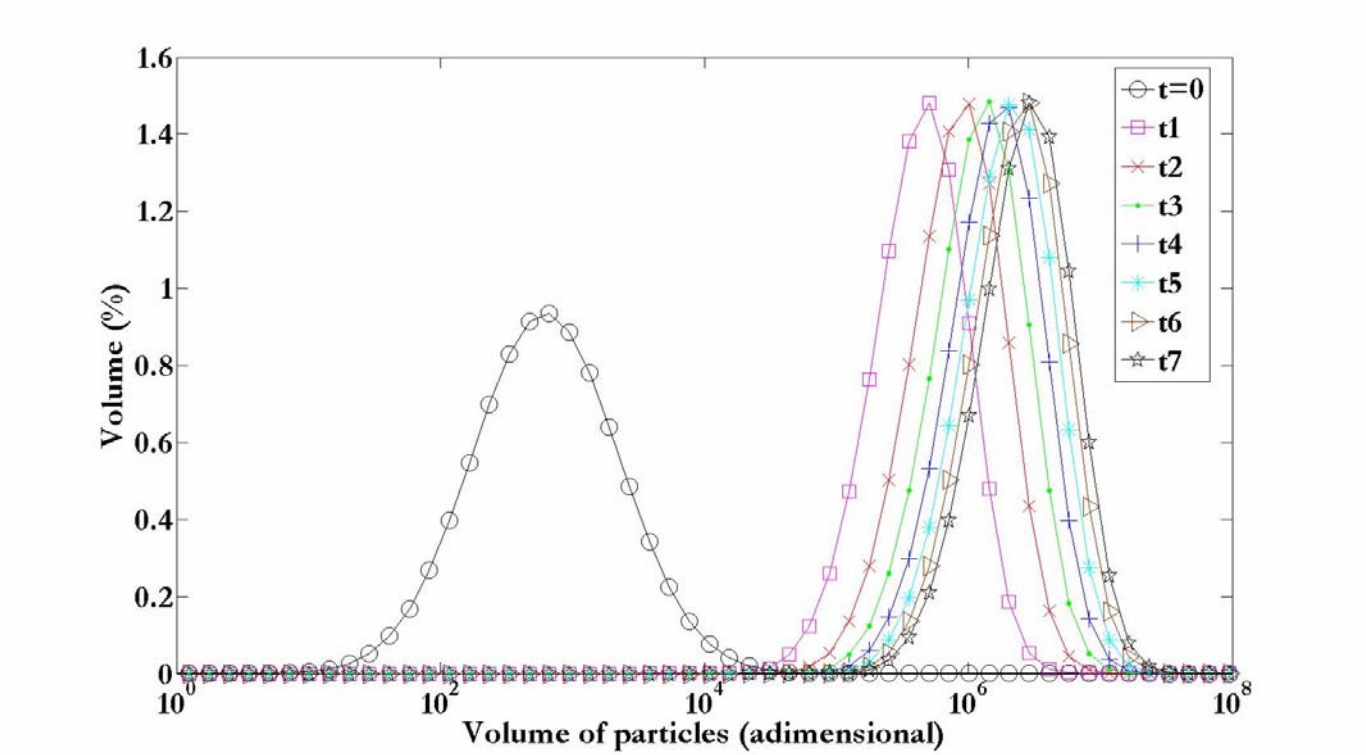
Volume (%)
Volume of particles (adimensional)
t=0
t1
t2
t3
t4
t5
t6
t7

**Fig.9**

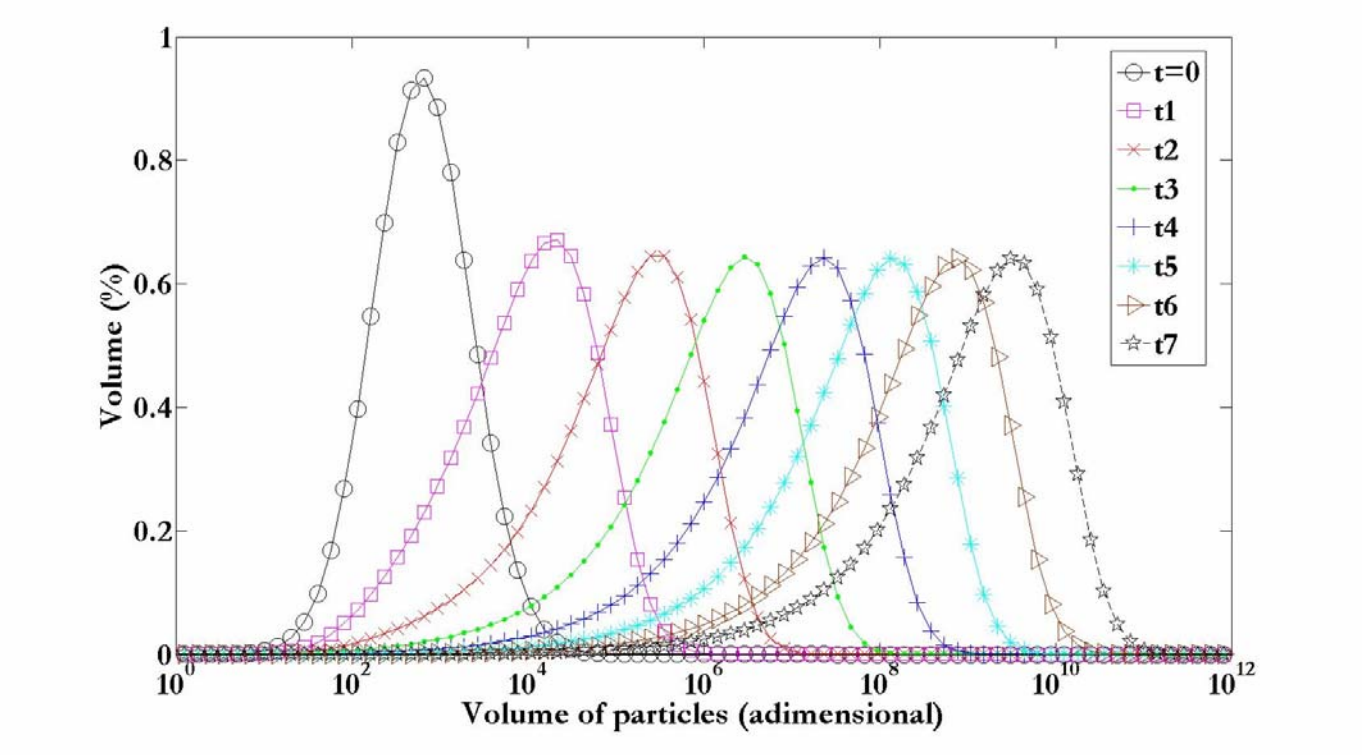
Volume (%)
Volume of particles (adimensional)
t=0
t1
t2
t3
t4
t5
t6
t7

**Fig.10**

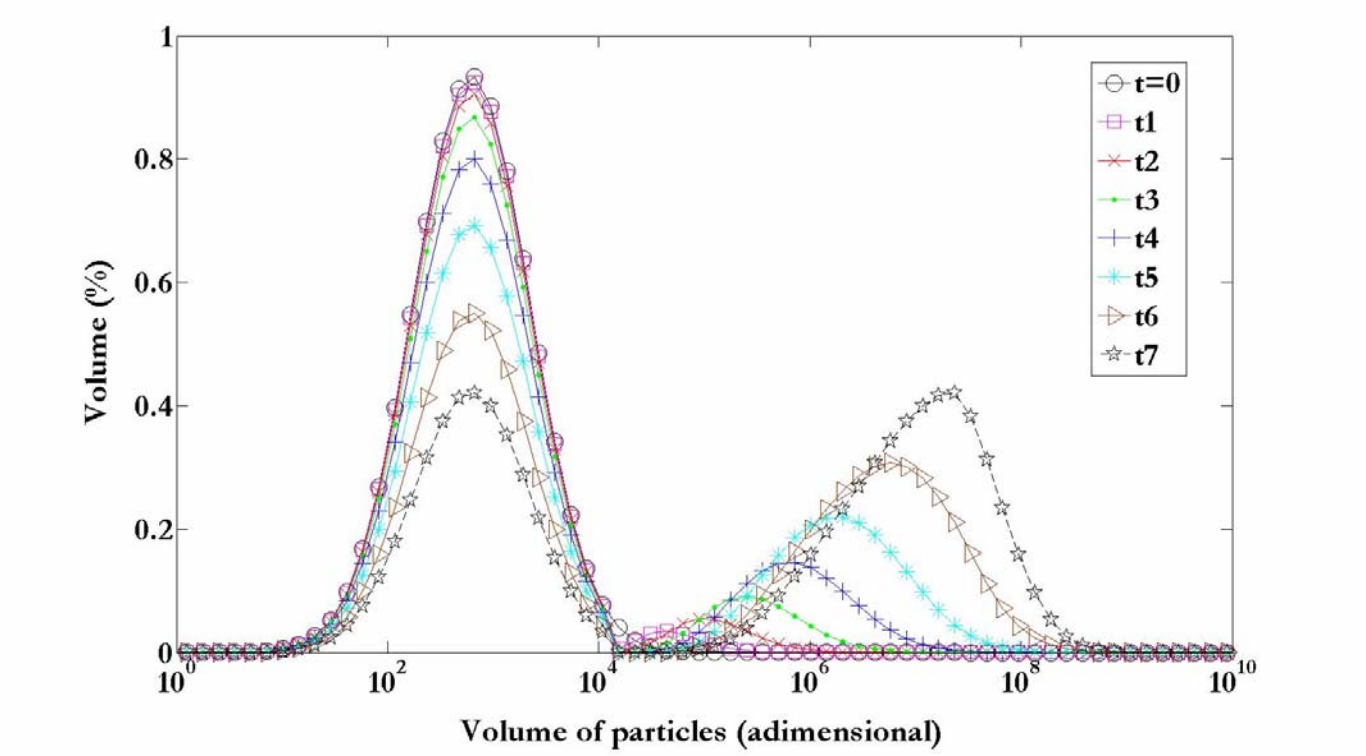
Volume (%)
Volume of particles (adimensional)
t=0
t1
t2
t3
t4
t5
t6
t7

**Fig.11**

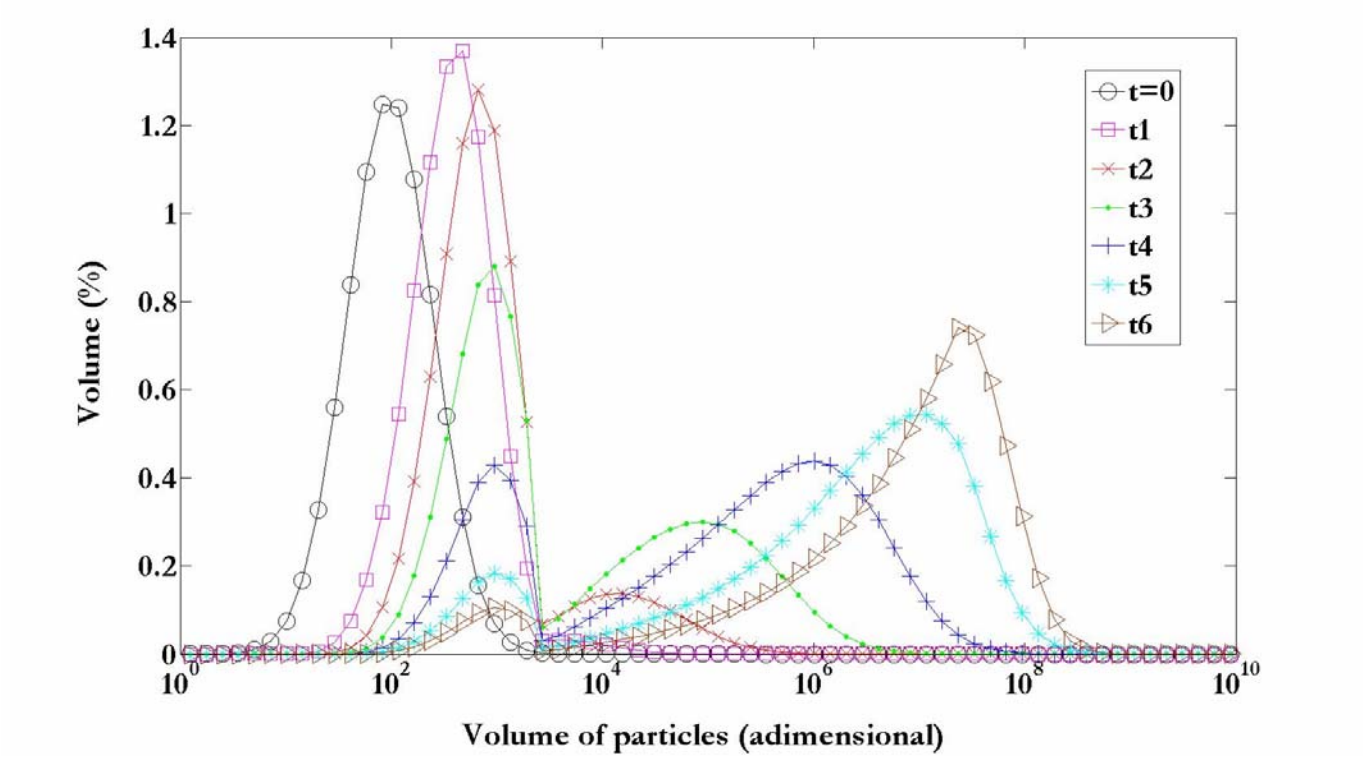


**Fig.12**

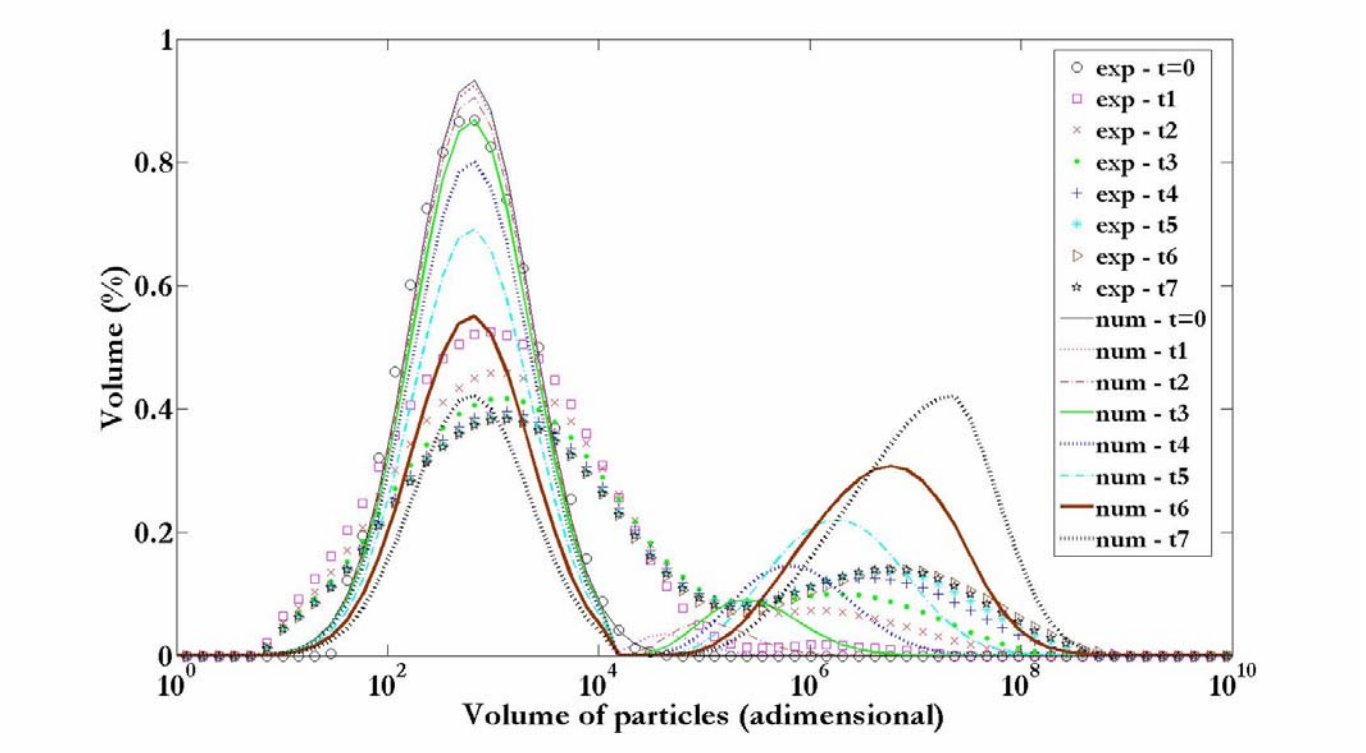
Volume (%)
Volume of particles (adimensional)
exp - t=0
exp - t1
exp - t2
exp - t3
exp - t4
exp - t5
exp - t6
exp - t7
num - t=0
num - t1
num - t2
num - t3
num - t4
num - t5
num - t6
num - t7

**Fig.13**

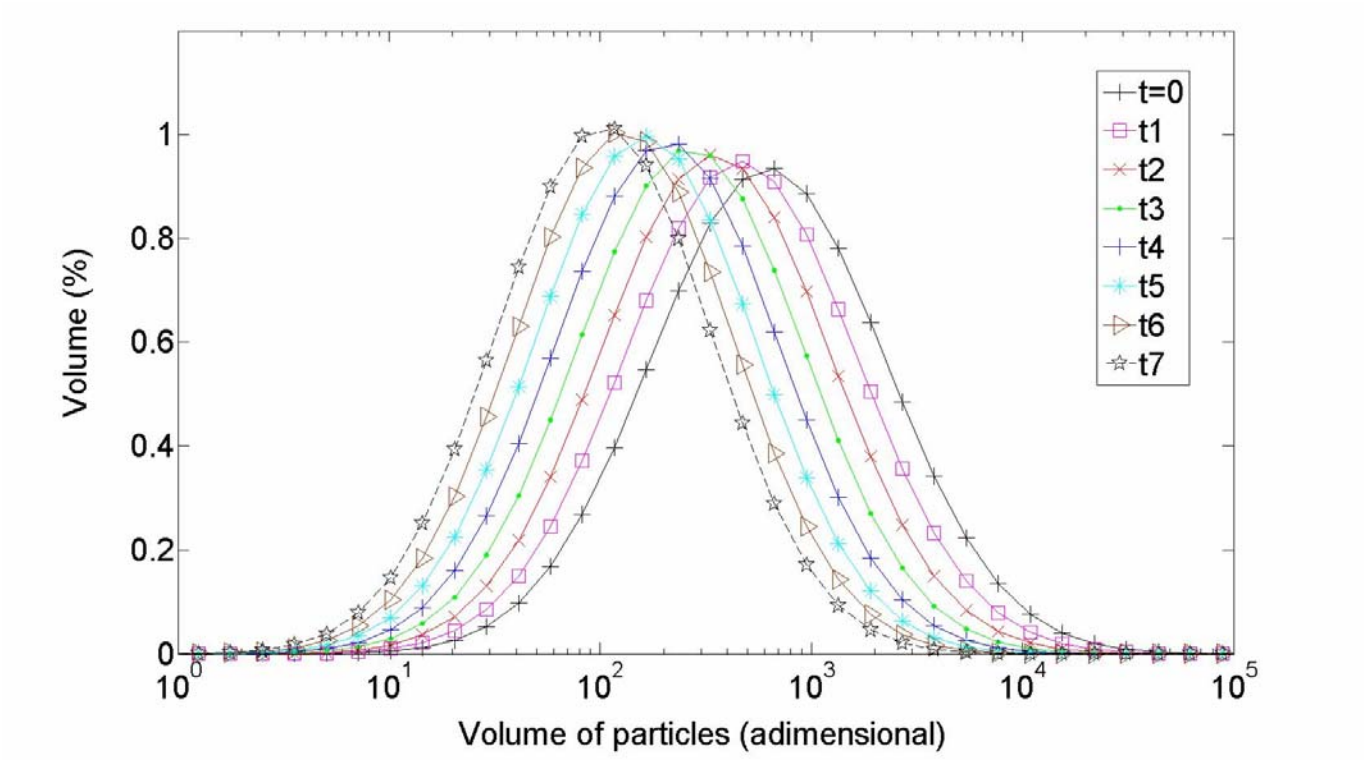
Volume (%)
Volume of particles (adimensional)
t=0
t1
t2
t3
t4
t5
t6
t7
0
0.2
0.4
0.6
0.8
1
10^0
10^1
10^2
10^3
10^4
10^5

**Fig.14**

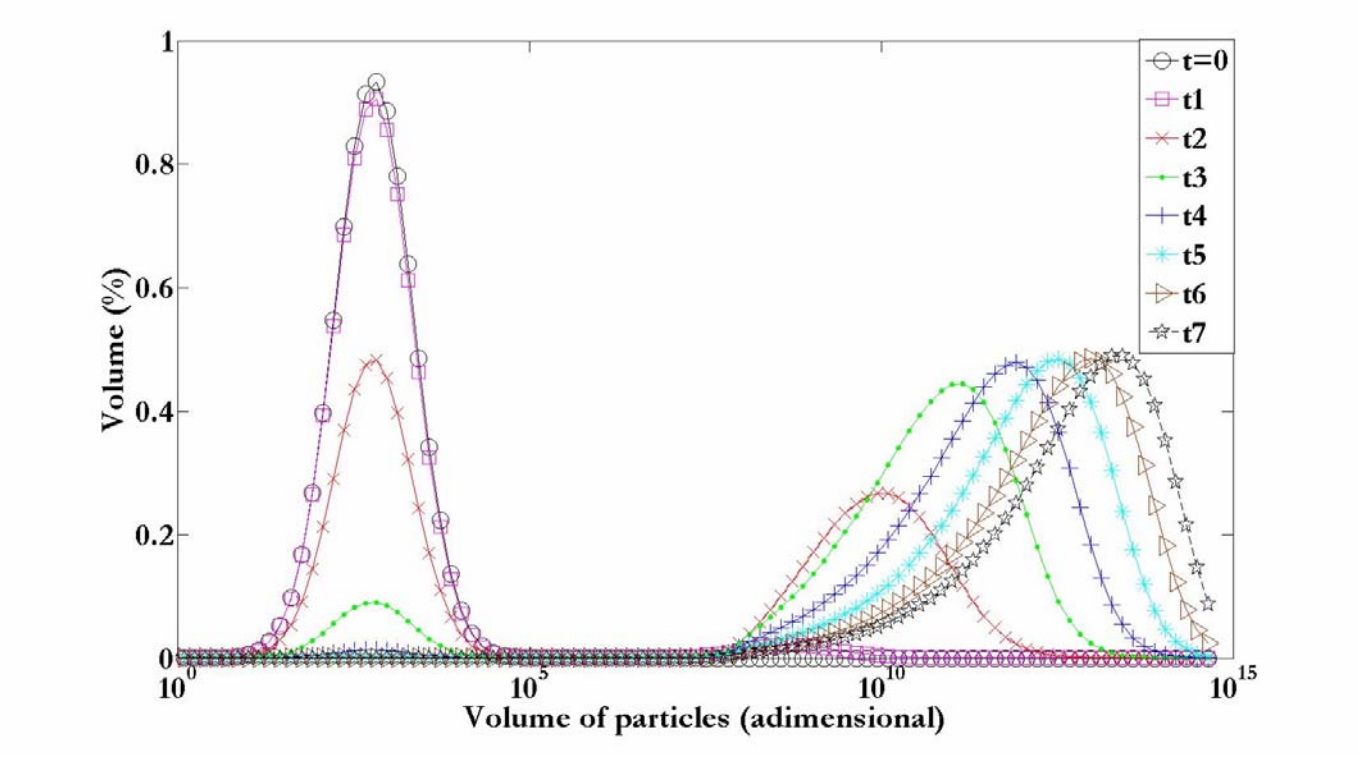
t=0
t1
t2
t3
t4
t5
t6
t7
Volume (%)
Volume of particles (adimensional)
0
0.2
0.4
0.6
0.8
1
10^0
10^5
10^10
10^15

**Fig.15**

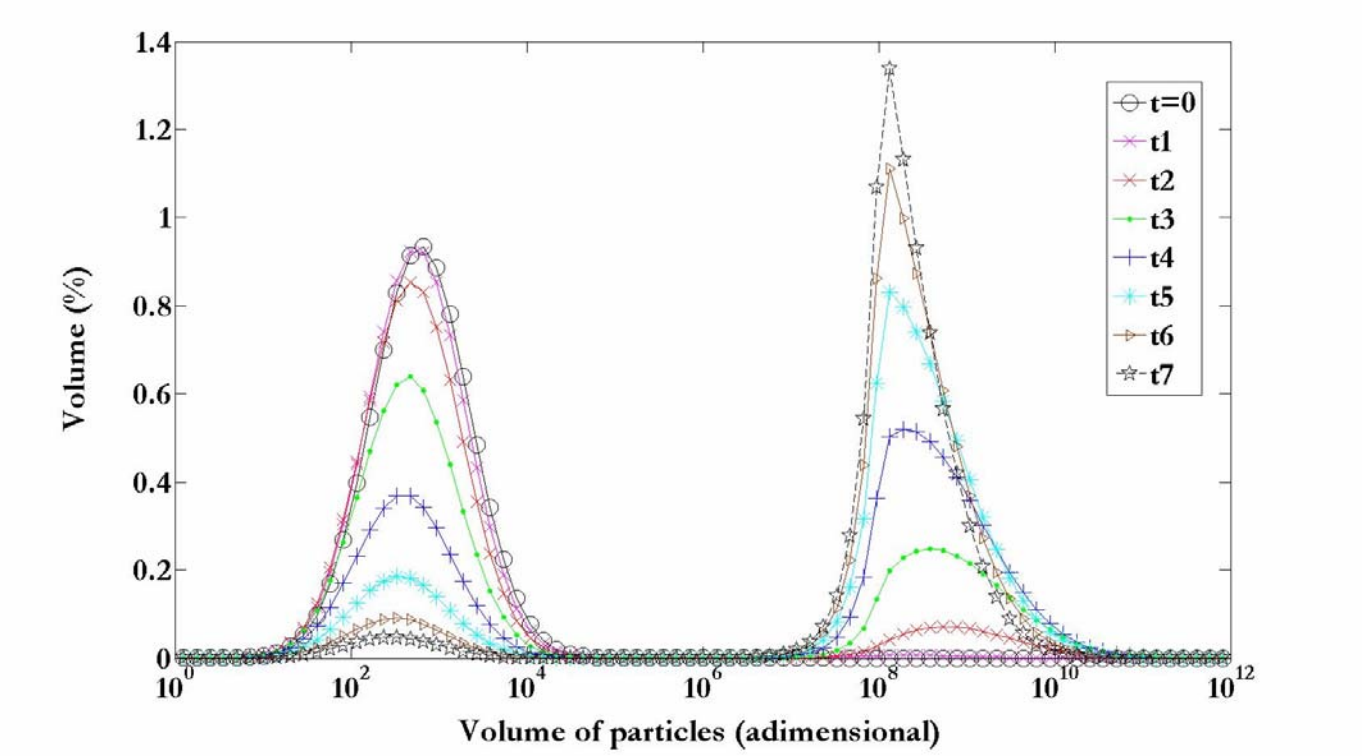
Volume (%)
Volume of particles (adimensional)
t=0
t1
t2
t3
t4
t5
t6
t7

**Fig.16**